Tellus (1996), 48A, 383–402
Printed in UK – all rights reserved

TELLUS
ISSN 0280–6495

A numerical case study of a polar low in the Labrador Sea

By J. MAILHOT[1,*], D. HANLEY[2,†], B. BILODEAU[1] and O. HERTZMAN[2], [1]*Recherche en Prévision Numérique, Atmospheric Environment Service, Dorval, Québec, Canada;* [2]*Department of Oceanography, Dalhousie University, Halifax, Nova Scotia, Canada*

(Manuscript received 19 April 1995; in final form 2 October 1995)

ABSTRACT

A mesoscale (15 km) version of the Canadian regional finite-element model is used to study a polar low that developed in the Labrador Sea on 11 January 1989, in the wake of an intense cold air outbreak associated with a major synoptic-scale system located to the east of Greenland. The rapid evolution of the polar low is well revealed from satellite imagery showing a complex structure with strong surface winds near the vortex and deep convection nearby during the mature stage. The simulated structure of the polar low agrees quite well with observed features. Based on the detailed mesoscale model outputs, the evolution of the Labrador Sea polar low is discussed at the initiation and mature stages. The polar low developed under a combination of baroclinic and convective processes. At an early stage, baroclinic development takes place in conditions of reversed shear flow, marked by low-level baroclinicity near the ice edge and a mobile upper-level short wave. Rapid modification of the Arctic boundary layer by strong surface heat fluxes is similar to that observed in other areas. Sensitivity experiments indicate that the mutual interaction between the upper-level potential vorticity anomaly and the low-level baroclinicity at the Arctic front, favored by the deep convective boundary layer, appears to trigger the polar low. At the onset of the mature stage, the approach of a cold air dome favors the outbreak of deep convection, in agreement with satellite imagery. As shown by sensitivity experiments, latent heat release from organized convection contributes to the major part of the rapid deepening of the polar low in its mature stage, and sea surface evaporation is the primary feeding mechanism for condensation processes. The structure of the polar low is characterized by a warm core due to the combined effects of warm air seclusion and diabatic heating. Comparisons with previously studied polar lows developing in similar conditions of reversed shear at other locations are discussed.

1. Introduction

Observational studies, especially since the advent of satellite imagery, have revealed a wide variety of cyclonic disturbances in polar air masses (see the reviews by Rasmussen (1983), and Businger and Reed (1989)). These systems, often referred to as "polar lows", include any small synoptic or subsynoptic cyclonic disturbances that form in cold airmass, poleward of major jet streams or frontal zones. Polar lows are usually found over oceans in winter, and are characterized by a comma- or spiral-shaped cloud pattern as they mature. They often develop a warm core, and sometimes a clear eye surrounded by vigorous cumulonimbus clouds and strong surface winds, as in tropical cyclones and hurricanes (Rasmussen, 1989; Nordeng and Rasmussen, 1992).

Businger and Reed (1989) suggested a classification of polar lows based on the diagnostics of common types of developments. Comma clouds

* Corresponding author.
† Current affiliation: Department of Atmospheric Science, State University of New York at Albany, Albany, New York, USA.

are associated with the short-wave/jet-streak type of polar low characterized by positive vorticity advection aloft, deep baroclinicity and weak surface fluxes. The Arctic-front type of polar low is associated with ice boundaries, shallow baroclinicity and strong surface fluxes; such conditions are found near the Greenland and Norwegian Seas, the Gulf of Alaska, and the Bering and Labrador Seas. Grønås and Kvamstø (1994) proposed an extension of this classification to also include in the Arctic-front category the contributions of upper-air disturbances and deep convection. A significant proportion of Arctic-front polar lows develop in conditions of reversed shear flow, where the storm motion (steering-level wind) is in a direction opposite to the thermal wind (Duncan, 1978; Grønås et al., 1987; Bond and Shapiro, 1991).

Several theories have been put forward to explain the development of polar lows. Traditionally, these have been divided into two approaches: one relying mostly on baroclinic instability effects, the other favoring CISK (conditional instability of the second kind), air-sea interaction instability (Emanuel and Rotunno, 1989) or similar heating mechanisms. Recent work has highlighted the fact that polar lows often occur in combination with upper-air forcing and lower-level temperature anomaly related to diabatic effects. Craig and Cho (1989) showed that spiraliform polar lows tend to be CISK-dominated while comma clouds are primarily of baroclinic origin. They also found that an initially baroclinic system could become CISK-dominated as surface fluxes of heat and moisture decrease the stability of the atmosphere and promote deep cumulus convection. Indeed, there is increasing evidence that many polar lows often develop in two stages: a baroclinic phase linked to a mobile upper-level trough followed by the rapid intensification of a low-level vortex by diabatic processes.

As discussed by Businger and Reed (1989), the forecasting of polar lows poses a challenging problem to numerical weather prediction models. This is due to the relatively coarse resolution of most models (as compared to the small scale of polar lows), to a lack of details in the initial conditions, and to uncertainties in parameterization schemes used for boundary-layer and convective processes. This is particularly true for the smaller-scale Arctic-front type of polar low. Several sensitivity studies with numerical models (Grønås et al., 1987; Nordeng, 1987; Langland and Miller, 1989; Nordeng et al., 1989; Roch et al., 1991) have shown that high horizontal resolution, accurate sea surface temperature and ice margin analyses, and appropriate convective parameterization schemes are important in the forecasting of polar lows.

While research on polar lows has been quite active in areas such as the Norwegian Sea, the Gulf of Alaska and the Bering Sea, it is only recently that several studies have focussed on polar lows in the Canadian Arctic waters, such as the Beaufort Sea, the Hudson Bay and the Labrador Sea (Parker, 1989; Roch et al., 1991; Richards and Hanley, 1991; Rasmussen and Purdom, 1992). Interestingly, the climatological study of Richards and Hanley (1991) identified a preferred genesis region for polar lows in the Labrador Sea just off the north coast of Labrador. In the present study a mesoscale (15 km) version of the Canadian regional finite-element (RFE) model is used to simulate the development of a polar low that occurred on 11 January 1989 in the Labrador Sea. Numerical forecasts of two polar low events over Hudson Bay and over the Davis Strait by Roch et al. (1991) confirmed the potential of the RFE model, given appropriate horizontal resolution and forcing fields such as sea ice, to forecast polar lows with some success. Therefore, mesoscale numerical models offer a unique opportunity to study polar lows and, in this work, we will use the high-resolution model output, in conjunction with available satellite imagery, to investigate in more detail various aspects of the evolution of a polar low over the Labrador Sea.

The paper is organized as follows. Section 2 gives a description of the numerical model and the experimental setup. A synoptic description of the polar low is provided in Section 3. The results from the numerical model are discussed and compared with satellite imagery in Section 4. In Section 5, the evolution of the Labrador Sea polar low is discussed based on the detailed model outputs. Summary and conclusions are given in section 6.

2. The numerical forecast model

The mesoscale numerical model used in this study is very similar to the operational version

(1992) of the RFE model. The main features of the RFE model are summarized in Table 1. A geographic reference map is given in Fig. 1.

The RFE model is an evolved version of that of Staniforth and Daley (1979), with a semi-Lagrangian treatment of advection (Tanguay et al., 1989). It is a hydrostatic primitive equation model defined on a polar-stereographic projection true at 60°N. The integration procedure is based on a semi-implicit time differencing with a semi-Lagrangian treatment of advection allowing a timestep of 200 s. The RFE model uses the implicit nonlinear normal-mode initialization described by Temperton and Roch (1991). The vertical coordinate is a terrain-following σ coordinate (pressure normalized by its surface value) with 23 levels, irregularly spaced to provide better resolution in the boundary layer. This is important since polar lows are known to be shallow systems. The variable-resolution horizontal grid has a uniform resolution of 15 km over the central part of the domain (refer to Fig. 2 for the location of the central domain). This portion of the model grid actually includes an area much larger than the region of the polar low development. As will be discussed in section 4, the development of the polar low was found to be sensitive to the proper forecast of a synoptic-scale low pressure system located to the east of Greenland.

Table 1. *Summary of the mesoscale RFE model*

Dynamics
hydrostatic primitive equations;
variable-resolution horizontal grid overlaid on a polar stereographic projection (15 km in central domain);
semi-implicit semi-Lagrangian (3-D) time integration (timestep of 200 sec);
23 σ levels (normalized pressure) with top at $\sigma_T = 0.01$ and high vertical resolution close to the surface;
linear finite elements in (x, y, σ);
explicit lid boundary condition $\dot{\sigma} = 0$ at σ_T;
linear ∇^2 horizontal diffusion of temperature, vorticity and divergence (terrain correction for T);
Physics
planetary boundary layer based on turbulent kinetic energy;
fully-implicit vertical diffusion;
stratified surface layer based on similarity theory;
prediction of surface temperature over land (force-restore method);
enhanced sea surface temperature analysis;
solar and infrared radiation fluxes calculated at all levels;
shallow convection parameterization;
Kuo-type convective parameterization;
grid-scale condensation in supersaturated layers.

Fig. 1. Geographic reference map of the study area. The numbers refer to the locations used in Table 2 for SSM/I and model comparisons of surface wind speeds.

Coupled to the dynamical model is a comprehensive set of parameterization of physical schemes (Benoit et al., 1989; Mailhot et al., 1989). These include a planetary boundary layer based on turbulent kinetic energy, a surface layer based on similarity theory, solar and infrared radiation, large-scale precipitation and a Kuo-type deep convection scheme. The current version also includes the modifications to the physics package described by Mailhot (1992), comprising revisions to the vertical diffusion scheme and the addition of a shallow convection parameterization.

The initial conditions for the 36-h forecasts of the polar low case are obtained by interpolation from the archived operational objective analyses of the Canadian Meteorological Centre (CMC).

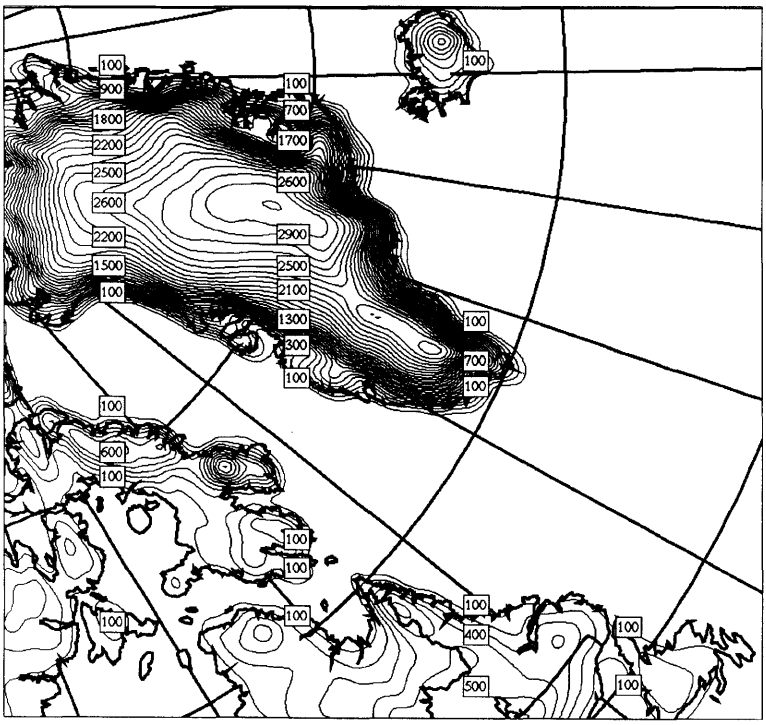

Fig. 2. The orography (contours every 100 m) used by the RFE model. The area corresponds to the central portion of the domain with uniform resolution (15 km).

Details on the objective analysis procedure can be found in Mitchell et al. (1990). The horizontal resolution of the data in the analysis is 2° in longitude and in latitude, thus the resulting resolution of the data supplied to the model is about 200 km over the area of the development. Because the data is at lower resolution than that of the model integrations, some time is required for the fields to adjust to the model resolution. Therefore, the forecasts are started approximately 24 h before maximum development occurred, as determined from observations and satellite imagery.

The topography field used by the model is shown in Fig 2. A number of features are relatively well represented. For instance, the Hudson Strait and the Torngat Mountains in northern Labrador are clearly defined, the Frobisher Bay and Cumberland Sound on Baffin Island are also well captured by the model. However, there are still some limitations to this orography field: although most areas of high elevation are well resolved, the model mountains are not quite high enough in comparison with the real orography.

As emphasized in numerous studies, polar lows are sensitive to variations in the sea surface temperature. Therefore, in order to get a good representation of the polar low development, a detailed sea surface temperature analysis obtained from the Canadian Forces Metoc Centre in Halifax is used in this study (Fig. 3). This high-resolution analysis is based on data from aircrafts, ships and buoys, and is updated about every four days. Over a large area in the middle of the Labrador Sea, the enhanced analysis shows a significant warm temperature anomaly (on the order of 5°C) when compared to climatology. This indicates that the ocean temperatures were much warmer than average during that period and, indeed, the climatology of Labrador Sea polar lows of Richards and Hanley (1991) confirms that 1989 was an exceptional year in terms of frequent outbreaks of polar lows. As will be seen in the next section, this

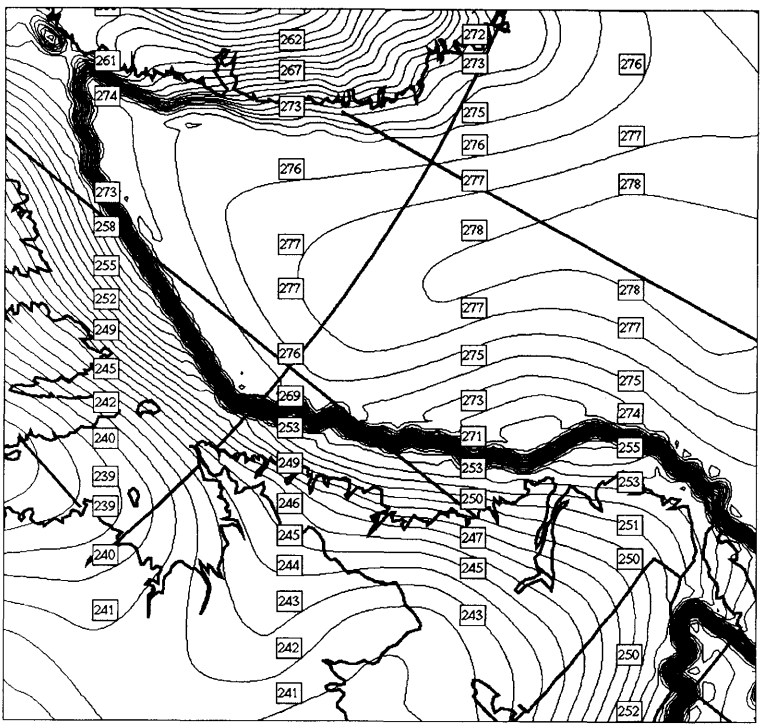

Fig. 3. Sea surface temperature analysis (contours every 1 K) and ice margin (thick contours) valid 10 January 1989.

region of anomaly corresponds well with the location of the polar low during its mature stage. Fig. 3 also shows the location of the ice margin obtained from the Canadian Forces Metoc Centre and satellite imagery. For the surface energy balance, grid points designated as being ice-covered (coverage $>50\%$) are treated as land-covered grid points. Surface sensible heat and vapor fluxes from the open waters are permitted only at ice-free or partially ($<50\%$) ice-free grid points.

3. Synoptic description

The case studied here occurred on 11 January 1989 in the Labrador Sea and appears as a typical example of polar low development in this area. This case has also been investigated by Rasmussen and Purdom (1992) who showed how data from several satellites (GOES 7, NOAA and DMSP), combined with the few available conventional meteorological data, can be useful to study polar lows in the absence of high-resolution data. Apart from the satellite imagery, the only other useful information to track the polar low over the area is a drifting buoy that was located near 51°W, 59.5°N.

Prior to the development of the polar low, an intense low pressure system associated with the baroclinic zone of the polar jet moved across the coast of Labrador on January 9 and stalled to the east of Greenland on 10 January. In the wake of the low, cold and dry continental air was advected across the Labrador Sea until 12 January. On January 10, another trough developed over Hudson Bay (Fig. 4), and the associated 500 hPa short wave moved over the Labrador Sea on January 11, with a dome of very cold air. In its central portion, the core of cold air reached temperatures of -47°C at 500 hPa, resulting in a weaker static stability of the atmospheric column favorable to the outbreak of deep convection. Clearly, this case fulfils the criteria proposed by Rasmussen et al. (1993) and Rasmussen and Cederskov (1994) for its classification as a primary polar low where surface development is associated

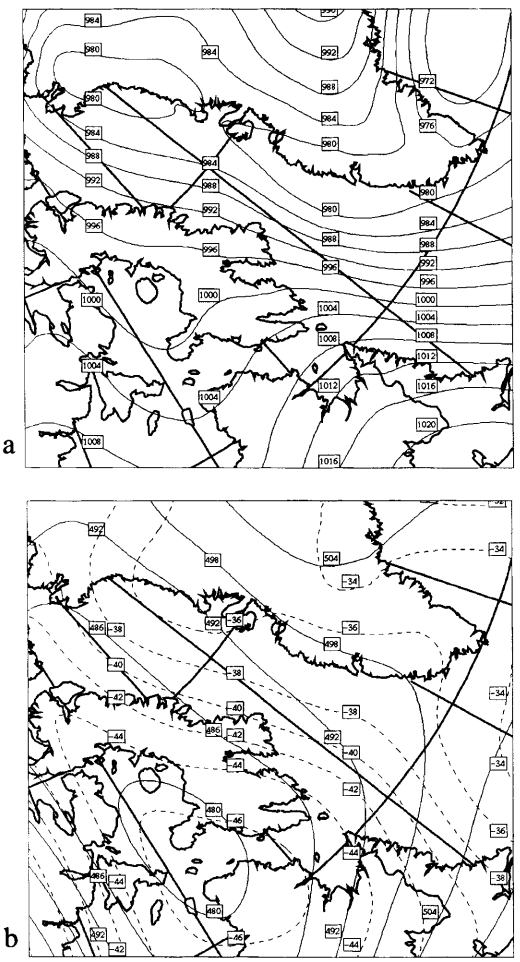

Fig. 4. Analysis valid at 1200 UTC 10 January 1989. (a) Mean-sea-level pressure (solid contours every 4 hPa); (b) 500 hPa geopotential height (solid, every 6 dam) and temperature (dashed, every 2°C).

with the dynamic forcing resulting when an upper-level cold-core vortex (with 500-hPa temperature below a threshold value of −42°C) crosses an ice edge.

The rapid evolution of the polar low is well revealed from the satellite imagery (Fig. 5). The polar low began to develop around 0600 UTC 11 January and reached a mature stage by 1800 UTC the same day. Shortly after reaching maturity, the polar low dissipated rapidly and, by 1200 UTC 12 January 1989, the polar low has completely disappeared. At the early stage of development, an extensive cirrus cloud field was present to the northeast of Labrador associated with flow over the Torngat Mountains of northern Labrador (not shown). The surface low forms immediately to the east of central Labrador with the outbreak of cold air from the continent marked by the leading Arctic front. The beginnings of a circulation centre was seen near 60°W, 58.5°N at the southern edge of the large cloud shield, with a line of clouds extending to the east, resembling a frontal zone. This line is located at the confluence of the northwesterly flow off Baffin Island and the westerly flow off Labrador, as inferred from the orientation of the cloud streamers. At 1211 UTC (Fig. 5a), the circulation becomes better defined and a small vortex centre is visible. Long cloud streets with a northwest-southeast orientation are found at the exit of Hudson Strait and Frobisher Bay, an indication of strong low-level winds associated with air circulation around a low pressure region. To the west of Greenland, the wind direction has shifted to the north. At this time, the drifting buoy reported a falling surface pressure with a value of 993.8 hPa.

At the mature stage (Fig. 5b), the main circulation centre located near 52°W, 58°N has developed a clear eye structure with a band of clouds wrapping around it. A line of cumulus clouds is found near Greenland, resulting from the northwesterly flow along the coast and the westerly flow further south. The subsynoptic analysis of Rasmussen and Purdom (1992) based on satellite imagery indicates a complex structure developing around the polar low at this time. The cloud track derived wind fields show wind velocities reaching 20 ms^{-1} south and southeast of the main vortex, and the development of a secondary circulation centre located further northwest (53°W, 60°N) with deep convection nearby (Rasmussen and Purdom, 1992; see their Fig. 2). They also noted that deep convection increased around the polar low during its mature stage. At 1700 UTC, the buoy had drifted to 50.5°W, 59°N and reported a surface pressure of 989.5 hPa falling rapidly. The buoy was then located about 100 km ahead of the approaching polar low. It is worth noting that this was indeed the last report received from the buoy, presumably destroyed in the strong gusty winds and high seas associated with the polar low complex. By 2201 UTC (Fig. 5c), the polar low approaches the southern coast of Greenland and begins to dissip-

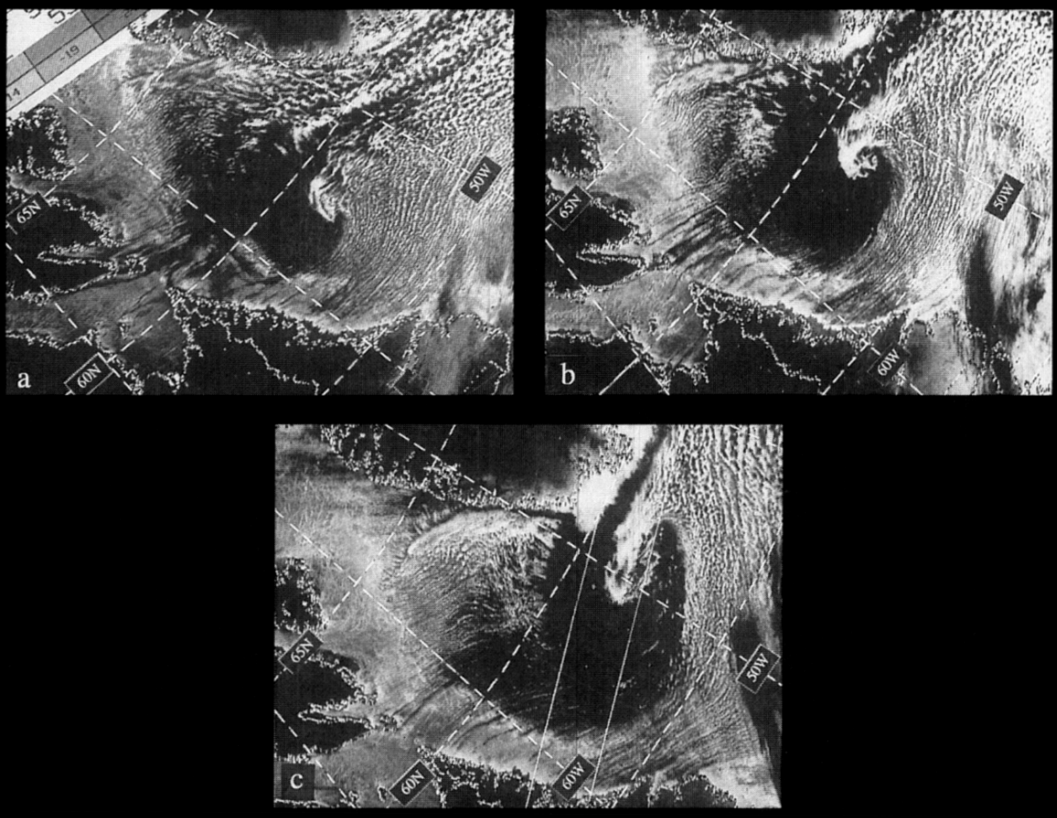

Fig. 5. Infrared imagery of the polar low from (a) NOAA 10 satellite valid at 1211 UTC 11 January 1989, (b) NOAA 11 satellite valid at 1652 UTC 11 January 1989, (c) NOAA 10 satellite valid at 2201 UTC 11 January 1989.

ate as the cold, dry and stably stratified glacial air is being advected into the polar low from the north. This air replaces the relatively warm, moist inflow air to the north of the low. The convection then quickly dissipates and the polar low gradually loses its structure and eye. Based on microwave SSM/I data, Rasmussen and Purdom (1992) reported that the eye area of the low has very little cloud water content by this time, while high cloud water content is present south of the vortex centre.

4. Model verification

The development of the polar low predicted by the model is shown in Fig. 6. The 18-h forecast valid at 0600 UTC 11 January 1989 (not shown) exhibits a pattern of short-wave troughs and ridges, resulting possibly from the combined effects of sea surface fluxes near the ice margin and lee troughing from the mountains of Baffin Island and the Torngat Mountains. The surface winds indicate a prevailing westerly flow over Labrador and a northwesterly flow off Baffin Island. Winds exiting the Hudson Strait reach values near 20 ms^{-1}, as air is accelerated over the ice margin into the area of lower pressure. The Hudson Strait may also act as a local wind channel resulting in enhanced low-level jets, and creating regions of strong horizontal wind shear conducive to low-level vorticity source. At 1200 UTC (Fig. 6a), a surface trough is present and is intensifying over the Labrador Sea. The polar low appears to develop along a convergence line extending eastwards along 60°N from the ice margin east of the coast of Labrador. This convergence line also coincides quite well with a line of maximum

absolute vorticity, and is visible in satellite imagery as a line of cumulus clouds (Fig. 5a). This feature was already present in the 12-h model forecast at 0000 UTC 11 January (not shown) and it intensified during the next 12 h. The convergence line forms as the northwestly flow off Baffin Island and Davis Strait meets the westerly flow to the east of Labrador.

An interesting feature is that the development takes place in an environment characterized by conditions of reversed shear flow. As indicated in Fig. 6a, the surface flow is northwesterly near the low-level trough and a closed low is present at upper levels with a southwestward tilt from the surface trough. Duncan (1978) showed that baroclinic development is favored in the region of reversed vertical shear. Such situations are characterized by cold air advection in the northwesterly flow, by strong surface winds implying an enhancement of surface energy fluxes and often by a warm core structure due to warm air seclusion by the cold air flow.

By 1800 UTC 11 January (Fig. 6b), the model has developed a more complicated pattern charac-

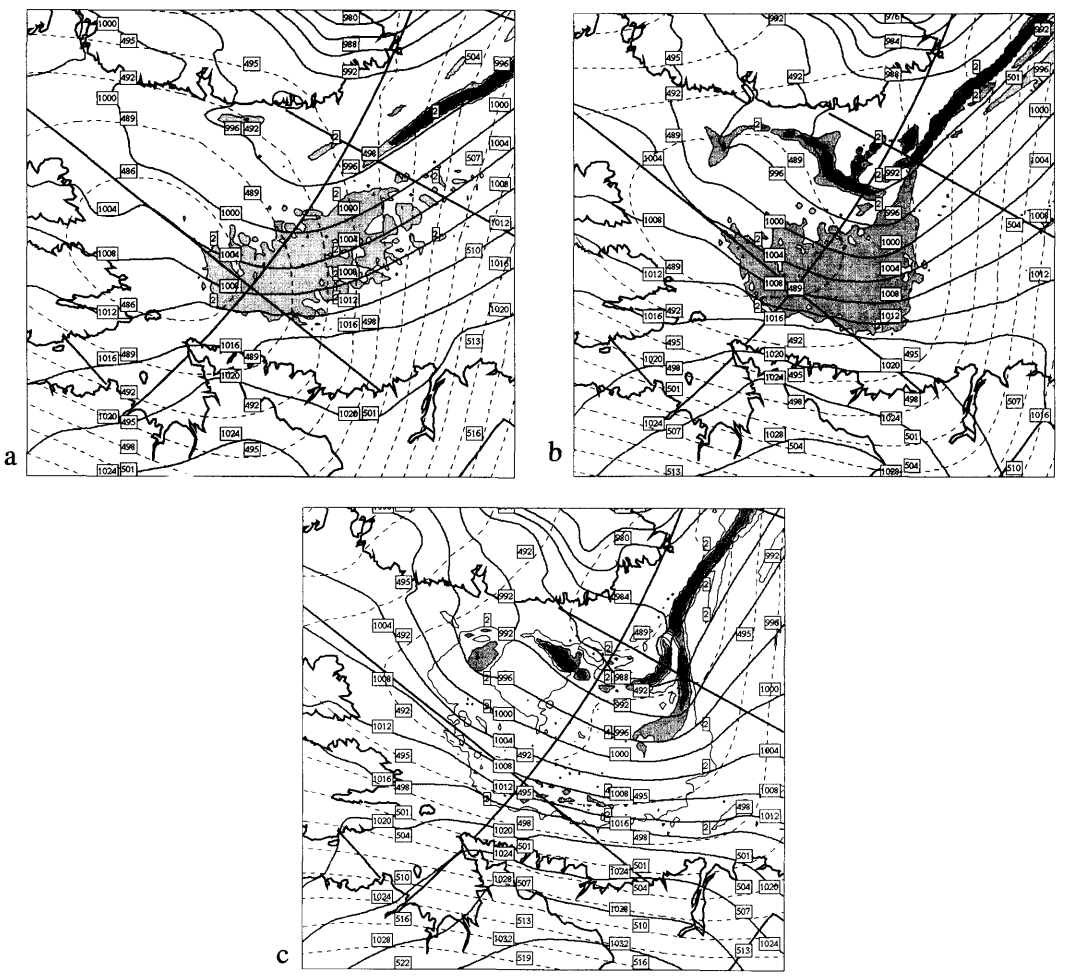

Fig. 6. Mean-sea-level pressure (solid contours every 4 hPa), 500 hPa geopotential height (dashed contours, every 3 dam) and precipitation rate (shaded contours, every 2×10^{-7} m s^{-1}) from (a) 24-h forecast valid at 1200 UTC 11 January 1989, (b) 30-h forecast valid at 1800 UTC 11 January 1989, (c) 36-h forecast valid at 0000 UTC 12 January 1989.

terized by a deeper surface trough and a main vortex with a central pressure of 990.5 hPa, and a secondary circulation located further northwest with a similar central value. This secondary low appears to be related to the outbreak of a vigorous convective activity on the fronts associated with the polar low. The precipitation pattern is organized in a typical frontal structure reminiscent of an extratropical storm, but at a smaller scale and inverted from the usual orientation. The surface pressure values over the area are in agreement with the last buoy report of 989.5 hPa. We note also that the predicted pattern bears some resemblance to the complex structure described by Rasmussen and Purdom (1992). The polar low complex deepened further to 983 hPa 6 h later (Fig. 6c). The tight pressure gradient results in strong winds across the Labrador Sea exceeding 25 ms^{-1} and produces a frontal structure quite similar to that seen in satellite imagery, giving the polar low system a comma shape (cf. Fig. 5c). Upward motion is taking place near and west of the surface low, as expected in a reversed shear flow, and also with the associated frontal structures and the convergence line. The satellite imagery showed the presence of deep convection at later stages of the polar low, an indication that convective heating also played a role in the intensification of the system. Indeed, areas of strong convection are present in the forecasts to the north and west of the polar low, and also along the convergence line extending east of the polar low (cf. Fig. 6b,c). The model precipitation is almost entirely convective, with no evidence of stratiform precipitation in the region of development.

Because the polar low developed in the northern part of the Labrador Sea, there are few conventional meteorological observations available to verify the model. Surface winds over the open ocean obtained from SSM/I constitute a useful and accurate data sample to study polar lows (Goodberlet et al., 1989; Claud et al., 1992). SSM/I derived surface wind speeds for 0813 UTC and 2204 UTC 11 January 1989 are compared in Table 2 with the model predicted surface winds at specific locations. Good agreement is obtained, with the winds underestimated by the model at locations 5 and 8 in the vicinity of the polar low, and some overestimation of winds at location 2. Note that part of these errors may be due to the incorrect positioning of the low too far to the north. Indeed, a close comparison with the satellite imagery reveals that the model develops the polar low further to the north than observed, but that the final position of the low at 0000 UTC 12 January is at nearly the right location.

Table 2. *Comparison of SSM/I derived and model surface wind speeds (in ms^{-1}); refer to Fig.1 for the locations*

		SSM/I	Model
0813 UTC			
	1	22–24	20
	2	6–8	11
	3	6–8	12
	4	20–22	21
	5	22–24	21
2204 UTC			
	6	18–20	17
	7	20–22	19
	8	22–24	17
	9	8–10	8
	10	22–24	22

A number of sensitivity experiments to horizontal resolution and sea surface temperature have been performed on this polar low case (Hanley, 1993). Generally, these experiments confirm the findings of previous studies (Grønås et al., 1987; Langland and Miller, 1989; Nordeng et al., 1989; Roch et al., 1991) that indicate that the polar low development is sensitive to the sea surface temperature, to the accurate location of the ice margin, and to the horizontal resolution. Some sensitivity to orographic forcing in the form of lee troughing off Baffin Island and Labrador was also noted. The possible strengthening effects due to orography from Greenland, Iceland and Spitsbergen mountains have been suggested in other studies (Grønås et al., 1987). Preliminary tests with the model also showed a sensitivity of the polar low development to the size of the central (high-resolution) part of our model domain. To achieve a realistic simulation of the polar low, it was found necessary to correctly handle the major synoptic-scale low located to the east of Greenland. Indeed, this synoptic system did not deepen enough when it was located outside of the high-resolution area. This resulted in a much weaker arctic air outbreak over the Labrador Sea and the polar low failed to

develop properly. We note that polar lows without this type of dependence upon synoptic-scale features have been successfully simulated with a smaller domain (Roch et al., 1991), suggesting that the horizontal extent of the model grid might be a limiting factor in simulating polar lows developing in cold air outbreaks associated with a large-scale synoptic system downstream.

In summary, the structure of the storm simulated by the model is found to be consistent with the available observations. It is also worth noting that the model storm travels at a rate comparable to the satellite observed polar low and exhibits similar frontal features. The model develops the polar low a bit too far to the north, but the final position is remarkably accurate. The discrepancies at the early stage of the development of the polar low may be due to the lack of details in the coarse initial conditions representative of an area with very few meteorological observations. Also, there may be significant limitations with some forcing fields. This suggests that, although the initial forcing in the model is apparently misplaced, the subsequent development of the polar low is mainly controlled by diabatic processes well handled by the model. In the next section, we use the unique high-resolution dynamically-consistent dataset provided by the model forecast to discuss in more detail the evolution and internal structure of this Labrador Sea polar low.

5. Discussion

It has been found difficult to formulate a general model of polar lows encompassing all types of development. Several models have been proposed on the basis of aircraft observations or numerical model results. Bond and Shapiro (1991) discussed a conceptual model based upon observations of a polar low in the Gulf of Alaska. The polar low developed in conditions of reversed shear within a mature, occluded synoptic-scale cyclone. Frontogenesis at low levels resulted from confluence and differential cold-air advection between the polar air stream to the west of the synoptic low and the warm air secluded near the core of the low. This development was primarily a baroclinic disturbance without significant convective contribution. The model of Bond and Shapiro was found to apply also to polar lows in the Bering Sea and the Norwegian Sea. Montgomery and Farrell (1992) devised a two-stage development model incorporating moist processes and strong baroclinic dynamics. This two-stage theory of polar low development is consistent with the idea that polar lows often develop under a combination of baroclinic and convective processes (Rasmussen, 1979; Nordeng, 1987; Businger and Reed, 1989) and, in this context, it has been suggested that polar low formation can be studied from a potential vorticity (PV) perspective (e.g. Grønås and Kvamstø, 1994).

5.1. *Initiation of the polar low*

A number of factors have been stressed in the development of many Arctic-front type of polar lows, including the role of heat and moisture fluxes from the underlying sea surface and the presence of a low-level tropospheric inversion in the Arctic boundary layer (Økland, 1989; Kahl et al., 1992). The capping inversion generally enhances the low-level convergence of heat by confining vertical mixing of heat in the storm environment to a shallow boundary layer. Deep convection is then inhibited by the strong inversion, except in the region directly underneath upper-air disturbances.

At 0000 UTC 11 January, a shallow baroclinic zone characterized by tight gradients of equivalent potential temperature at low levels (Fig. 7a) is present along the ice edge off Labrador, with westerly to southwesterly winds. The patterns of surface fluxes of sensible (Fig. 7a) and latent heat (Fig. 7b) indicate intense fluxes near the ice margin at the exit of Hudson Strait and east of Labrador, in association with strong winds and the deepening of the surface trough. The maximum values reach 1400 Wm^{-2} for the sensible heat flux, while smaller values of 500 to 600 Wm^{-2} are found for the latent heat flux. These compare with values for combined fluxes of 1000 Wm^{-2} reported by Shapiro et al. (1987) in a case of polar low over the Norwegian Sea, and of the order of 1500 Wm^{-2} in a similar case of polar low development in the Labrador Sea (Rasmussen et al., 1993) . The dominance of the sensible heat flux over the latent heat was noted by Roch et al. (1991) as typical of arctic conditions, with relatively small moisture content due to the cold temperature. However, as noted by Albright et al. (1994), this evaporation flux represents a huge amount of

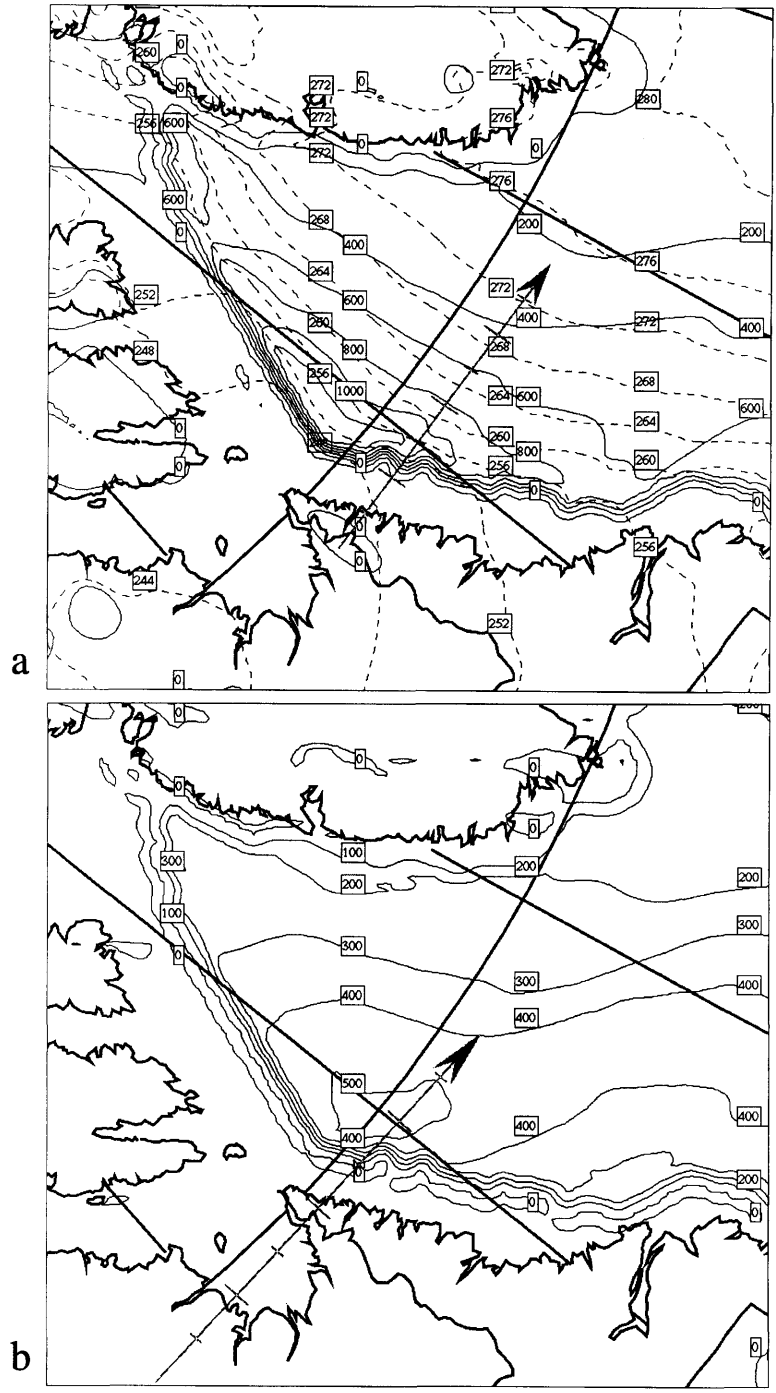

Fig. 7. 12-h forecast valid at 0000 UTC 11 January 1989 of (a) surface sensible heat flux (solid contours every 200 Wm^{-2}) and 925 hPa equivalent potential temperature (dashed contours, every 4 K), (b) surface latent heat flux (contours every 100 Wm^{-2}). Arrow in (a) and (b) shows the location of the section in Figs. 8 and 9, respectively.

moisture added to the atmosphere and available for condensation processes. As the cold air is advected across the ice margin over warmer waters, the air begins to warm and moisten in response to surface heating and evaporation. This is well depicted in the vertical cross-sections through the Arctic front (Fig. 8), showing the rapid modification of the Arctic boundary layer structure due to the strong surface fluxes and the rising of the top of the convective boundary layer reaching around 650 hPa. A stratocumulus cloud layer is forming at the top of the boundary layer. The instability can be seen in satellite imagery as streamers and cumulus cloud streets over the water (cf. Fig. 5). The cloud deck gradually thickens leading eventually to local areas of deep convection. The frontal structure of this Arctic cold air outbreak seems quite typical and shows many similarities with Arctic fronts observed at other locations (e.g. Shapiro and Fedor, 1989; see their Fig. 5).

At the initiation stage, the PV perspective suggests that the mutual interaction between an approaching upper-level PV anomaly and a low-level thermal anomaly can provide the necessary mechanism to spin-up the polar low. The existing low-level anomaly can be the result of several processes, including differential heating from sea

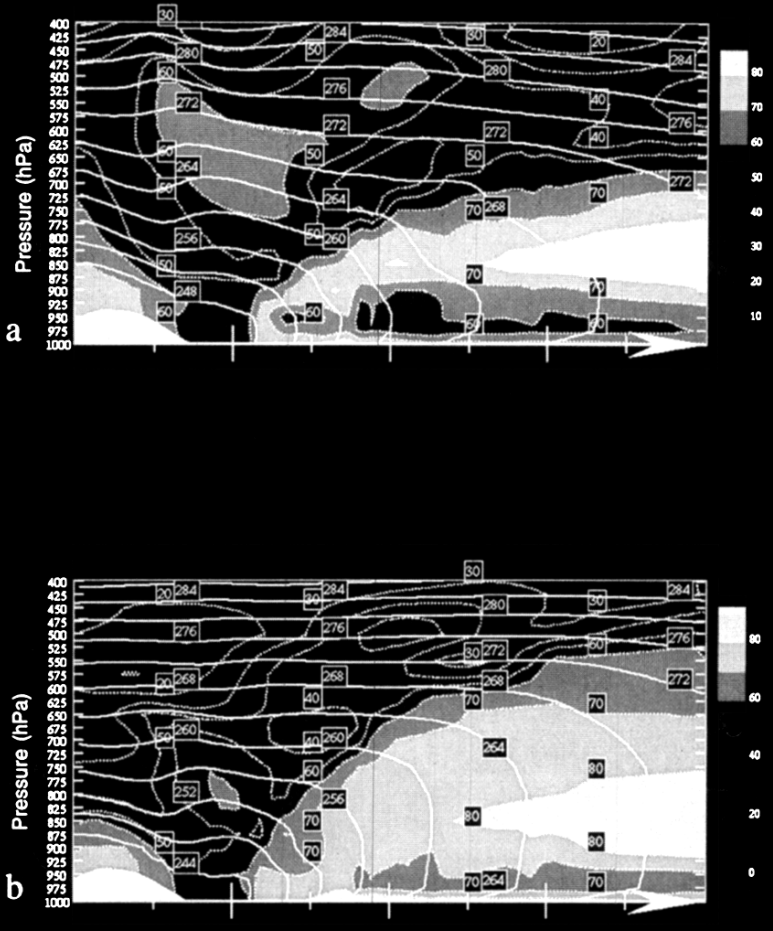

Fig. 8. Vertical cross-section (along baseline indicated in Fig. 7a) of potential temperature (solid, every 4 K) and relative humidity (dashed and shaded, every 10%) for (a) 12-h forecast valid at 0000 UTC 11 January 1989, (b) 24-h forecast valid at 1200 UTC 11 January 1989. Vertical axis is pressure (in hPa).

surface fluxes and tongues of warm air within an occluded system (Grønås et al., 1987). The surface temperature perturbation may also be induced by the upper-level anomaly itself provided the Rossby penetration height is large enough (Grønås and Kvamstø, 1994). In the present case, the upper-level PV anomaly (Fig. 9a) is related to a 700 hPa short-wave trough with an associated vorticity maximum situated to the east of northern Labrador. The approaching upper-level PV anomaly reaches down to 750 hPa at this time. Another region of PV anomaly is present at lower levels below 800 hPa at the top of the stably-stratified boundary layer and extends across the ice edge over the open sea surface. This low-level PV anomaly is similar to the structure obtained from aircraft observations by Shapiro and Fedor (1989; see their Fig. 6b) across the ice margin west of Spitsbergen associated with the secondary circulation at an ice-edge boundary layer front. Also, there is marked ascending motion in the rising convective boundary layer ahead of the PV anomalies. These conditions are quite similar to those described by Grønås and Kvamstø (1994) as necessary conditions for the formation of polar lows in the Norwegian and Barents Seas. In such cases, the strong mutual interaction between an approaching PV anomaly aloft and a surface temperature anomaly is favored by the small vertical separation between the base of the upper-level PV intrusion and the top of the deep convective boundary layer.

To assess the role of the sea surface fluxes and the PV anomalies in the initiation of the polar low, a sensitivity run was done by switching off the surface sensible heat flux. The low-level PV anomaly shown in Fig. 9a appears to be strongly linked to the boundary layer front at the ice edge, as this is not a prominent feature of the sensitivity run without sea surface heating (Fig. 9b). Furthermore, the main difference with the control run is that the boundary layer over the sea surface remains very shallow with subsidence above it; the separation with the upper-level PV anomaly is then increased, thereby not favoring the PV amplification mechanism. Indeed, no polar low development occurred in this sensitivity run. Therefore, in the present case, the major role of the surface heating from the ocean appears to be the quick transformation of the shallow, stably stratified Arctic boundary layer into a deep convective boundary layer, and the generation of a zone of strong low-level baroclinicity that can interact with the PV anomaly aloft.

Clearly, the initiation of the polar low is the result of a combination of factors. Considering the discrepancies in the initial location of the development, the model diagnostics cannot clarify completely the exact coupling mechanisms, but it is clear that a deep convective boundary layer, a significant low-level thermal anomaly and an upper-level PV anomaly all present simultaneously are important to initiate the development, in agreement with the scenario described by Grønås and Kvamstø (1994). Since the intensification of the incipient polar low generally took place in an area of strong sea surface heating, this highlights the significance of air-sea interactions in the development of the polar low. Furthermore, the importance of determining the exact location of these fluxes with accurate sea surface temperature and ice cover analyses is reiterated.

5.2. *Mature polar low*

As discussed in sections 3 and 4, at the onset of the mature stage, deep convection breaks out and a complex structure is generated characterized by a main vortex and the rapid development of a secondary circulation driven by convection. The outbreak of deep convection corresponds well with the arrival of the core of cold air at 500 hPa and the upper-level short-wave trough from the west (Fig. 10 and Fig. 6b). A pool of very cold air reaching $-49°C$ at 500 hPa allows deep convection to develop as it moves over the polar low, in agreement with the arguments of Økland (1989). At 36 h, the cold dome of air is located directly over the polar low, thus allowing deep convection to continue. However, by this time the short-wave trough has moved to the east of the polar low, a condition not conducive to further development and, indeed, this signals the end of the mature stage of the polar low and the beginning of its decay.

The structure of the polar low complex at the mature stage is depicted in the north-south cross-sections through the polar low (Fig. 11; refer to Fig. 10 for the location). In order to concentrate on the structure of the polar low itself, the sections do not include the secondary circulation found northwest of the polar low. The main cyclonic

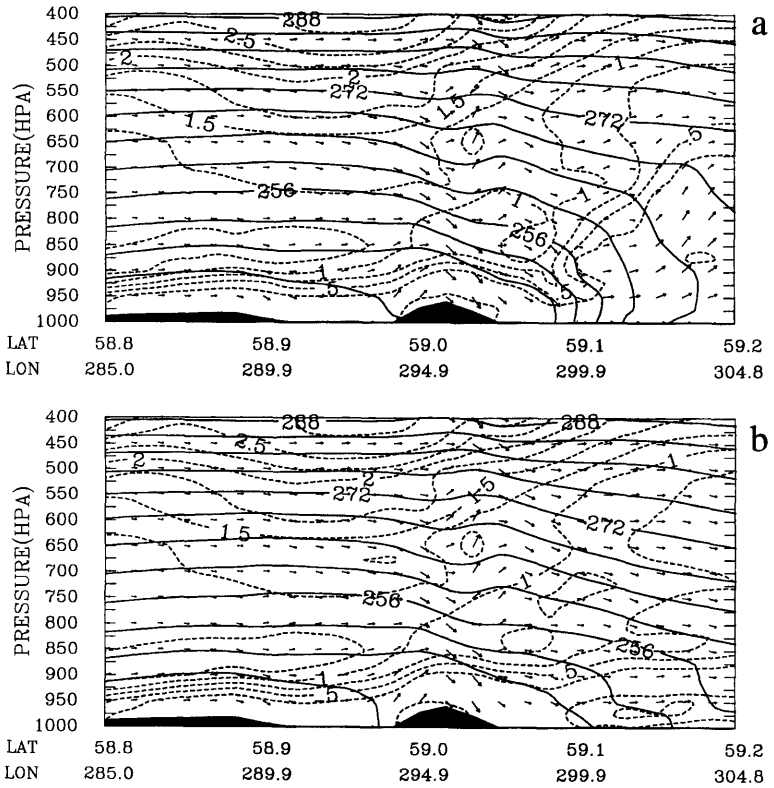

Fig. 9. Vertical cross-section (along baseline indicated in Fig. 7b) of potential temperature (solid, every 4 K) and potential vorticity (dashed, every 0.25×10^{-5} K hPa^{-1} s^{-1}) for 12-h forecast valid at 0000 UTC 11 January 1989 of (a) the control run and (b) the run without surface sensible heat flux. Vertical axis is pressure (in hPa) and vectors denote circulation along the section.

vortex is characterized by a maximum value of 43×10^{-5} s^{-1} at 950 hPa and reaches up to 500 hPa with anticyclonic vorticity aloft and almost no tilt in the vertical (Fig. 11a). Another vortex with a maximum value of 30×10^{-5} s^{-1} at 900 hPa and confined below 650 hPa is present further to the south. The vertical circulation pattern (Fig. 11b) indicates strong ascending motion above the polar low with a maximum at 750 hPa and weak subsidence just to the south. There is a region of significant sinking motion with a maximum at 800 hPa just to the north of the polar low, and upward motion further to the south associated with the surface trough. Dry areas (Fig. 11c) have begun to appear on either side of the polar low in these subsidence zones, especially to the north. The polar low structure is also characterized by a warm core with a temperature anomaly reaching a few degrees below 700 hPa (Fig. 11d). The warm core extends down from 600 hPa with a funnel shape and very slight northward tilt in the vertical. Here, strong upward motion is connected to the warm core, in contrast to tropical cyclones where subsidence is often present. Both the potential temperature and the equivalent potential temperature structures suggest a seclusion of a warm air core with the dry areas corresponding to the subsident cold air wrapping around the surface low.

The circulation with respect to the moving polar low is described in Fig. 12 (to highlight the relative circulation, the translation speed of the polar low estimated at about 9 ms^{-1} has been subtracted from the wind component perpendicular to the cross-section). Clearly, the air is swirling around the polar low over most of the troposphere. The

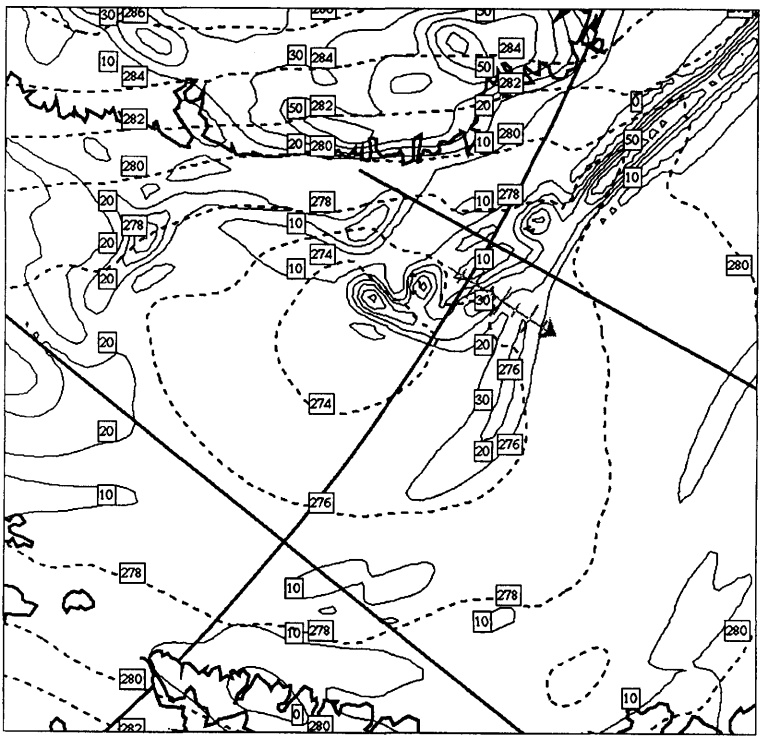

Fig. 10. 30-h forecast valid at 1800 UTC 11 January 1989 of 900-hPa absolute vorticity (solid, every 10×10^{-5} s^{-1}) and 500 hPa potential temperature (dashed, every 2 K). Arrow shows the location of the section in Figs. 11, 12.

relative circulation immediately to the north of the storm is easterly with winds reaching 5 ms^{-1}, and there is inflow at lower levels and outflow near 500 hPa. Just south of the polar low the circulation is westerly with a maximum of 5 ms^{-1} near 950 hPa. This jet enhances the vorticity of the system by adding cyclonic shear vorticity to its north side and also forces the cloud band to wrap around the southern edge of the polar low centre. Directly over the polar low, the horizontal relative flow is almost quiescent. Another westerly jet is present further south with a maximum of 10 ms^{-1} around 925 hPa. The upward motion in this area is associated with the surface trough in the reversed shear flow. Warm air seclusion occurs as the jet pushes cold air into the relatively warm air to the east of the polar low and surrounds a region of warm air, cutting it off from the warm source. Most of the air brought into the polar low is entrained at low levels from its northern side, and this air has been warmed during a long passage over open water along the west coast of Greenland. The entrainment of this warm air also enhances the convection to the northwest of the polar low. Finally, diabatic heating from intense convection is present near the polar low and is also a factor in the warming of the low centre. Therefore, it appears that the formation of the warm core results from a combination of warm air seclusion and diabatic heating.

In order to better isolate the role of diabatic effects in the development of the polar low, the model was run in a "dry" mode where the condensation processes (both the convective and grid-scale schemes) are by-passed but the surface fluxes are retained. The "dry" run only produces a weak and shallow trough. As indicated in Fig. 13, the condensation processes (especially the deep convection as discussed before) contribute to the major part of the rapid deepening of the polar low in its mature stage. Indeed, the condensation processes account for an additional surface deepening of 9 hPa (from 1000 to 991 hPa) after 30 h of simulation. In addition, the warm core is

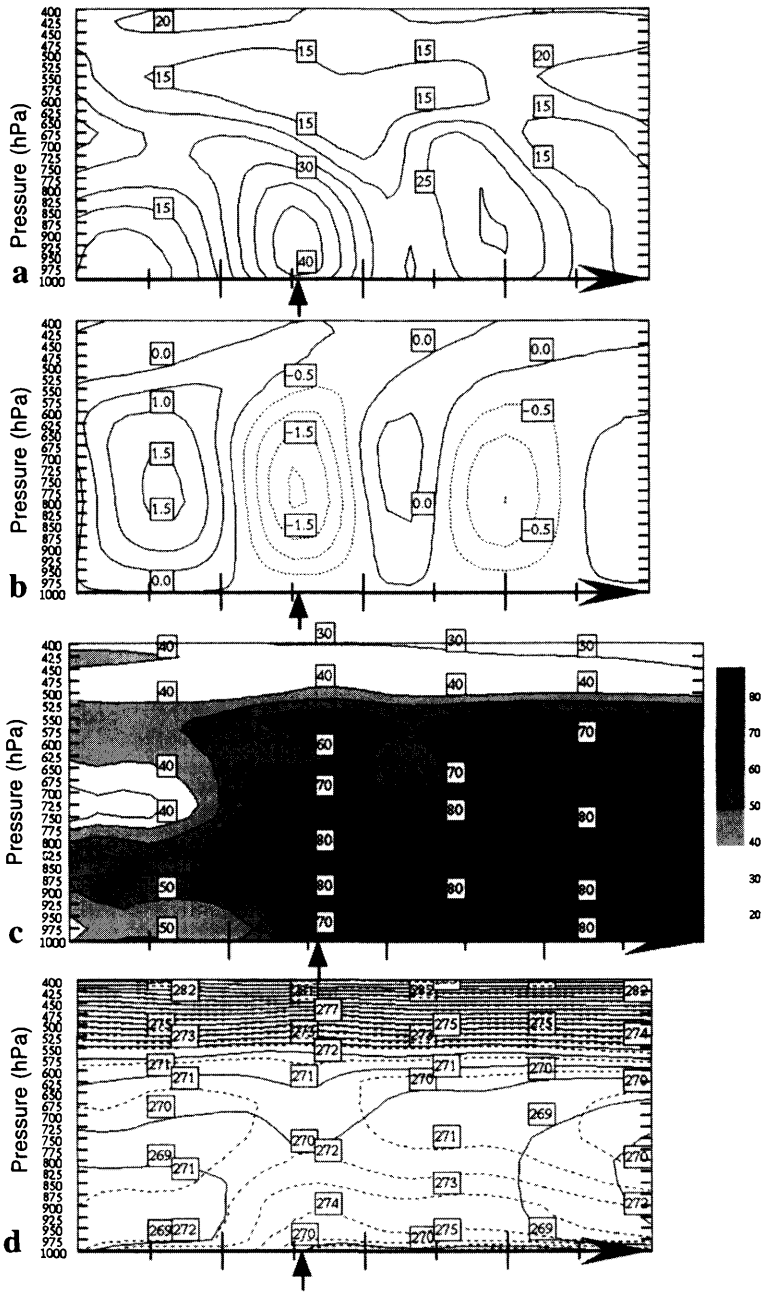

Fig. 11. Vertical cross-section (along baseline indicated in Fig. 10) for 30-h forecast valid at 1800 UTC 11 January 1989 of (a) absolute vorticity (solid, every 5×10^{-5} s^{-1}), (b) vertical motion (every 0.5 Pa s^{-1}, dashed upward motion, solid downward motion), (c) relative humidity (solid, every 10%), (d) potential temperature (solid, every 1 K) and equivalent potential temperature (dashed, every 1 K). Vertical axis is pressure (in hPa) and arrows at the bottom locate the polar low.

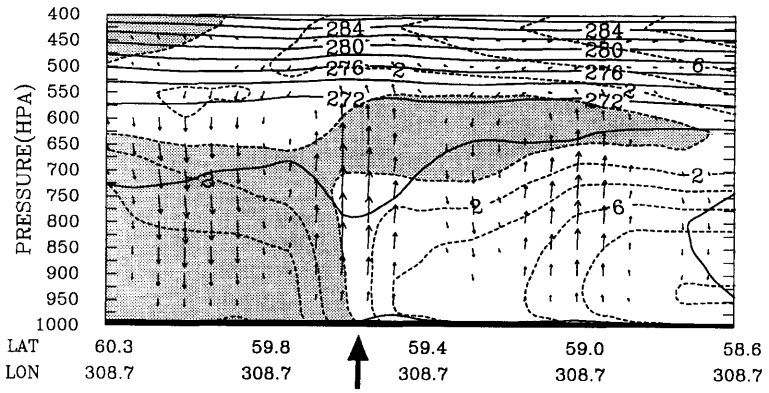

Fig. 12. Vertical cross-section (along baseline indicated in Fig. 10) for 30-h forecast valid at 1800 UTC 11 January 1989 of potential temperature (solid, every 2 K) and wind component across the section (dashed, every 2 m s^{-1}, and relative to moving polar low, negative values are shaded). Vertical axis is pressure (in hPa), vectors denote circulation along the section and arrow at the bottom locates the polar low.

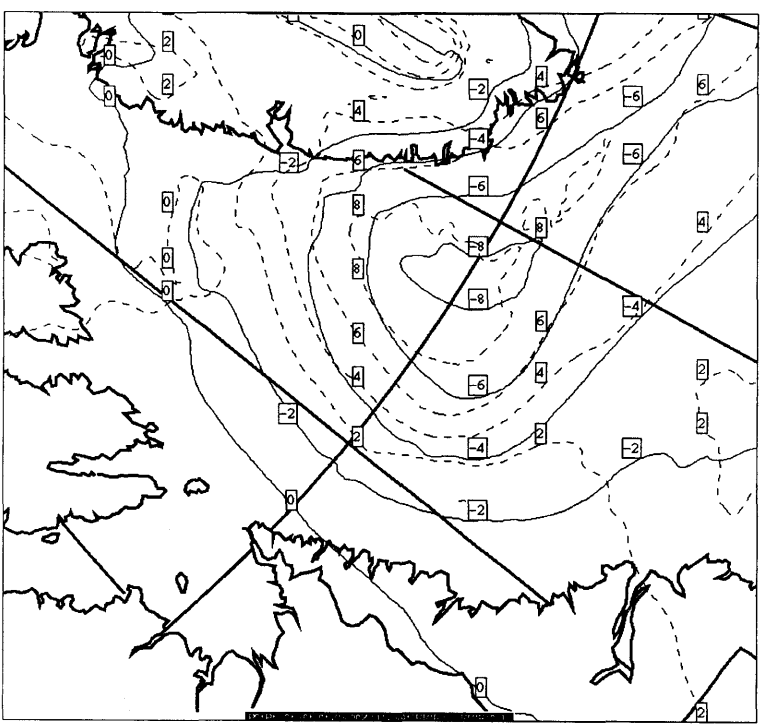

Fig. 13. Difference of mean-sea-level pressure (solid contours every 2 hPa) and 700 hPa potential temperature (dashed contours, every 2 K) between 30-h forecast valid at 1800 UTC 11 January 1989 of control run and "dry" run (no condensation processes).

absent in the "dry" run; large potential temperature differences between the "dry" run and the control run are present above and at the rear of the surface low centre and reach almost 10 K in a layer extending from the surface to 500 hPa. Therefore, one might argue that the warm core is a direct consequence of the latent heat release from condensation processes, but it may also be

an indirect result of the stronger circulations around the polar low producing a more vigorous warm air seclusion.

Interestingly enough, another sensitivity experiment where only the evaporation from the sea surface was turned off yielded results which are remarkably similar to the "dry" run. In particular, there is very little precipitation associated with the weak trough after 30 h of simulation (not shown). This confirms the major role of the outbreak of convection in the rapidly deepening phase of the polar low. Furthermore, this sensitivity experiment also indicates the importance of the strong sea surface fluxes in the rapid modification of the cold Arctic air mass and points out to the primacy of the surface evaporation fluxes as the main feeding mechanism for the condensation processes, in agreement with the findings of Roch et al. (1989) and Albright et al. (1994).

This polar low development over the Labrador Sea shows several similarities with other polar lows studied elsewhere. It bears some resemblance to the model discussed by Bond and Shapiro (1991) in the Gulf of Alaska. The present polar low also developed in conditions of reversed shear. However, in contrast to Bond and Shapiro, the development did not take place within, but at some distance at the rear of a mature, occluded synoptic-scale cyclone. In our case, the development was marked by a significant contribution from organized deep convection. The case studied here shows more striking similarities with some polar low cases in the Norwegian Sea studied by Grønås et al. (1987) and Grønås and Kvamstø (1994), characterized by a baroclinic development in a reversed shear flow forming an initial low in synoptic conditions favorable to trigger CISK-like mechanisms that further deepen the polar low with a warm occlusion. It also presents many resemblances with a polar low over the Davis Strait that Roch et al. (1991) compared to a scaled-down (to mesoscale) synoptic storm with a characteristic frontal structure.

6. Summary and conclusions

A mesoscale (15 km) version of the RFE model has been used to study a case of polar low development that occurred in the Labrador Sea on 11 January 1989. The selected case developed in association with an intense cold arctic air outbreak in the rear of a major synoptic-scale cyclone that stalled east of Greenland. It represents a typical polar low over the area associated with a short wave aloft and a dome of very cold air favorable to the outbreak of deep convection. The rapid evolution of the polar low occurred over less than 24 h and was well revealed from the satellite imagery showing a complex structure with strong surface winds near the vortex and deep convection nearby during the mature stage.

Based on the detailed mesoscale model outputs, the evolution of the Labrador Sea polar low was discussed in two stages corresponding to the initiation and mature stages. The polar low developed under a combination of baroclinic and convective processes. At the early stage, baroclinic development took place in conditions of reversed shear flow. Strong sea surface fluxes from the relatively warm waters of the Labrador Sea gave rise to the rapid modification of the Arctic boundary layer. Consequently, a stratocumulus cloud layer formed at the top of the rising convective boundary layer that gradually thickened. The frontal structure of this Arctic cold air outbreak was quite typical and showed many similarities with Arctic fronts observed in other areas. The PV perspective indicated that the interaction between an approaching upper-level PV anomaly and low-level baroclinicity associated with the Arctic front was favored by a deep convective boundary layer; this could provide the necessary mechanism to spin-up the polar low, in agreement with the scenario proposed by Grønås and Kvamstø (1994). The importance of a deep convective boundary layer and a low-level thermal anomaly in the triggering of the polar low was confirmed by a sensitivity experiment without surface heating from the ocean. At the onset of the mature stage, the cold air dome approaches the storm and deep convection breaks out as the polar low rapidly intensifies. Therefore, it appears that the necessary conditions for the operation of some CISK-like process were also present in this case. The precipitation pattern was organized in a typical frontal structure reminiscent of an extratropical storm, but at a smaller scale and inverted from the usual orientation, and was almost entirely convective. The structure of the polar low is characterized by a warm core extending below 500 hPa with a funnel shape due to the combined effects of warm air seclusion by

cold air wrapping around the surface low and diabatic heating from intense convection. Sensitivity experiments without condensation processes produced only a weak and shallow trough and indicated that latent heat release from organized deep convection contributed to the major part of the rapid deepening of the polar low in its mature stage. A sensitivity experiment without sea surface evaporation confirmed the major role of deep convection in the polar low development and the primacy of surface evaporation as the feeding mechanism for condensation processes.

Similarities of this case of polar low development over the Labrador Sea with previous studies of polar lows developing in similar conditions of reversed shear at other locations were discussed. The case studied here is similar to polar lows in the Norwegian Sea (Grønås et al., 1987; Grønås and Kvamstø, 1994) characterized by a baroclinic development in a reversed shear flow; the initial low further deepens in synoptic conditions favorable to trigger CISK-like mechanisms with a warm occlusion. The present case is also similar to a polar low over the Davis Strait (Roch et al., 1991) resembling to a mesoscale synoptic storm with a characteristic frontal structure.

Satellite imagery proved to be a useful source of data for model verification in the absence of a dense network of conventional meteorological observations over the region, providing a picture of the storm, indicating the timing of development and the structure of the polar low, and the presence of deep convection. The structure simulated by the model in the mature stage of the polar low is in a remarkably good agreement with available observations from satellite imagery and exhibits similar frontal features. The comparison with the satellite imagery revealed that the model develops the polar low further to the north than observed, but that the final position of the low is at nearly the right location. This is consistent with the fact that, although the initial forcing in the model is apparently misplaced, the subsequent development of the polar low is mainly controlled by diabatic processes well handled by the model. In agreement with several previous investigations, this highlights the capability of current numerical models, with appropriate physics and mesoscale resolution, of forecasting systems on the scale of polar lows with some success.

7. Acknowledgements

Thanks are due to Michel Béland for initiating this collaborative research between AES/RPN and Dalhousie University's Atmospheric Science Program. The research was partly based upon the M. Sc. thesis work of D. Hanley, under the supervision of O. Hertzman, with financial support from NSERC (Natural Science and Engineering Research Council) and PERD (Panel on Energy Research and Development).

The manuscript benefitted from the useful comments of André Tremblay and Michel Roch and the constructive criticisms of an anonymous reviewer. Vivian Lee provided her assistance in the preparation of the figures and in performing some of the model runs.

REFERENCES

Albright, M. D., Reed, R. J. and Ovens, D. W. 1994. Numerical simulations of a polar low over Hudson Bay. Proceedings, *International Symposium on the Life Cycles of Extratropical Cyclones*, 27 June-1 July 1994, Bergen, Norway, Vol. III, 3–8.

Benoit, R., Côté, J. and Mailhot, J. 1989. Inclusion of a TKE boundary layer parameterization in the Canadian regional finite-element model. *Mon. Wea. Rev.* **117,** 1726–1750.

Bond, N. A. and Shapiro, M. A. 1991. Polar lows over the Gulf of Alaska in conditions of reverse shear. *Mon. Wea. Rev.* **119,** 551–572.

Businger, S. and Reed, R. J. 1989. Cyclogenesis in polar air masses. *Wea. Forecasting* **4,** 133–156.

Claud, C., Katsaros, K. B. Petty, G. W. Chedin A. and Scott, N. A. 1992. A cold air outbreak over the Norwegian Sea observed from the TIROS-N Operational Vertical Sounder (TOVS) and the Special Sensor Microwave/Imager (SSM/I). *Tellus* **44A,** 100–118.

Craig, G. and Cho, H.-R. 1989. Baroclinic instability and CISK as the driving mechanisms for polar lows and comma clouds. *Polar and arctic lows.* Twitchell, P. F. Rasmussen, E. A. and Davidson, K. L. (eds.). A. Deepak Publishing, 131–140.

Duncan, C. N. 1978. Baroclinic instability in a reversed shear flow. *Meteor. Mag.* **107,** 17–23.

Emanuel, K. A. and Rotunno, R. 1989. Polar lows as arctic hurricanes. *Tellus* **41A,** 1–17.

Goodberlet, M. A., Swift, C. T. and Wilkerson, J. C.

1989. Remote sensing of ocean surface winds with the Special Sensor Microwave/Imager. *J. Geophys. Res.* **94** (C10), 14547–14555.

Grønås, S., Foss, A. and Lystad, M. 1987. Numerical simulations of polar lows in the Norwegian Sea. *Tellus* **39A**, 334–353.

Grønås, S. and Kvamstø, N. G. 1994. Synoptic conditions for Arctic front polar lows. Proceedings, *International Symposium on the Life Cycles of Extratropical Cyclones*, 27 June-1 July 1994, Bergen, Norway, Vol. III, 89–95.

Hanley, D. E. 1993. *A case study of a polar low in the Labrador Sea.* MSc thesis, Dept.of Oceanography, Dalhousie University, Halifax, Canada. 165 pp.

Kahl, J. D., M. C. Serreze ans R. C. Schnell, 1992. Tropospheric low-level temperature inversions in the Canadian Arctic. *Atmosphere-Ocean* **30**, 511–529.

Langland, R. H. and Miller, R. J. 1989. Polar low sensitivity to sea surface temperature and horizontal grid resolution in a numerical model. *Polar and arctic lows.* Twitchell, P. F. Rasmussen, E. A. and Davidson K. L. (eds.). A. Deepak Publishing, 247–254.

Mailhot, J. 1992. Numerical simulation of air mass transformation over the Gulf of Mexico. *J. Appl. Meteor.* **31**, 946–963.

Mailhot, J., Chouinard, C. Benoit, R. Roch, M. Verner, G. Côté J. and Pudykiewicz, J. 1989. Numerical forecasting of winter coastal storms during CASP: Evaluation of the regional finite-element model. *Atmos.-Ocean* **27**, 27–58.

Mitchell, H. L., Charette, C. Chouinard, C. and Brasnett, B. 1990. Revised interpolation statistics for the Canadian data assimilation procedure: their derivation and application. *Mon. Wea. Rev.* **118,** 1591–1614.

Montgomery, M. T. and Farrell, B. F. 1992. Polar low dynamics. *J. Atmos. Sci.* **49,** 2484–2504.

Nordeng, T. E. 1987. The effect of vertical and slantwise convection on the simulation of polar lows. *Tellus* **39A**, 354–375.

Nordeng, T. E., Foss, A. Grønås, S. Lystad, M. and Midtbø, K. H. 1989. On the role of resolution and physical parameterization for numerical simualtions of polar lows. *Polar and arctic lows.* Twitchell, P. F. Rasmussen E. A. and Davidson K. L. (eds.). A. Deepak Publishing, 217–232.

Nordeng, T. E. and Rasmussen, E. A. 1992. A most beautiful polar low. A case study of a polar low development in the Bear Island region. *Tellus* **44A**, 81–99.

Økland, H. 1989. On the genesis of polar lows. *Polar and arctic lows.* Twitchell, P. F. Rasmussen, E. A. and Davidson, K. L. (eds.). A. Deepak Publishing, 179–190.

Parker, M. N. 1989. Polar lows in the Beaufort Sea. *Polar and arctic lows.* Twitchell, P. F. Rasmussen, E. A. and Davidson, K. L. (eds.). A. Deepak Publishing, 323–330.

Rasmussen, E. A. 1979. The polar low as an extratropical CISK disturbance. *Quart. J. Roy. Meteor. Soc.* **105**, 531–549.

Rasmussen, E. A. 1983. A review of mesoscale disturbances in cold air masses. *Mesoscale meteorology: theories, observations and models.* Lilly, D. K. and Gal-Chen, T. (eds.). Reidel Publishing, 247–283.

Rasmussen, E. A. 1989. A comparative study of tropical cyclones and polar lows. *Polar and arctic lows.* Twitchell, P. F. Rasmussen, E. A. and Davidson, K. L. (eds.). A. Deepak Publishing, 47–80.

Rasmussen, E. A. and Purdom, J. F. 1992. Investigations of a polar low using geostationary satellite data. Preprints, *6th Conference on Satellite Meteorology and Oceanography*, 5–10 January 1992, Atlanta, Georgia, USA, Amer. Meteor. Soc., 120–122.

Rasmussen, E. A., Turner, J. and Twitchell, P. F. 1993. Report of a workshop on applications of new forms of satellite data in polar low research. *Bull. Amer. Meteor. Soc.* **74**, 1057–1073.

Rasmussen, E. A. and Cederskov, A. 1994. Polar lows: A critical appraisal. Proceedings, *International Symposium on the Life Cycles of Extratropical Cyclones*, 27 June-1 July 1994, Bergen, Norway, Vol. III, 199–203.

Richards, W. and Hanley, D. 1991. *Polar lows in atlantic Canadian waters.* Contract No. AEST 304–404.

Roch, M., Benoit, R. and Parker, N. 1991. Sensitivity experiments for polar low forecasting with the CMC mesoscale finite-element model. *Atmos.-Ocean* **29**, 381–419.

Shapiro, M. A. and Fedor, L. S. 1989. A case study of an ice-edge boundary layer front and polar low development over the Norwegian and Barents Seas. *Polar and arctic lows.* Twitchell, P. F. Rasmussen, E. A. and Davidson, K. L. (eds.). A. Deepak Publishing, 257–277.

Shapiro, M. A. L. S. Fedor and Hampel, T. 1987. Research aircraft measurements of a polar low over the Norwegian Sea. *Tellus* **39A**, 272–306.

Staniforth, A. N. and Daley, R. W. 1979. A baroclinic finite-element model for regional forecasting with the primitive equations. *Mon. Wea. Rev.* **107**, 107–121.

Tanguay, M., Simard, A. and Staniforth, A. N. 1989. A three-dimensional semi-Lagrangian scheme for the Canadian regional finite-element forecast model. *Mon. Wea. Rev.* **117**, 1861–1871.

Temperton, C. and Roch, M. 1991. Implicit normal mode initialization for an operational regional model. *Mon. Wea. Rev.* **119**, 667–677.